

Supplementary information

Nanozyme-Reinforced Injectable Photodynamic Hydrogel for Combating Biofilm Infection

Junqing Zhang^a, Shuang Zhao^a, Shen Zhang^a, Hao Zhu^a, Yaoxin Zhang^a, Linpei Li^a,
Chaoqun Liu^{*a,b}, Jiahua Shi^{*a}

^a School of Pharmacy, Key Laboratory of Natural Medicine and Immune-Engineering of Henan Province, Henan University, Kaifeng, 475004, P. R. China.

^b Department of Pharmacy, the First Affiliated Hospital of Henan University, Kaifeng, 475001, P. R. China.

E-mail: cqliu@henu.edu.cn, sjiahua@henu.edu.cn

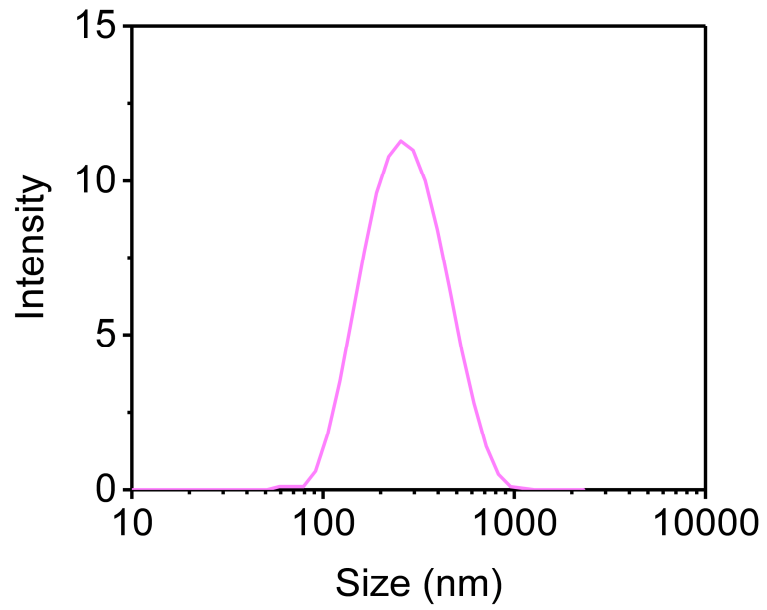


Fig. S1 Size distribution of MnO₂ NS.

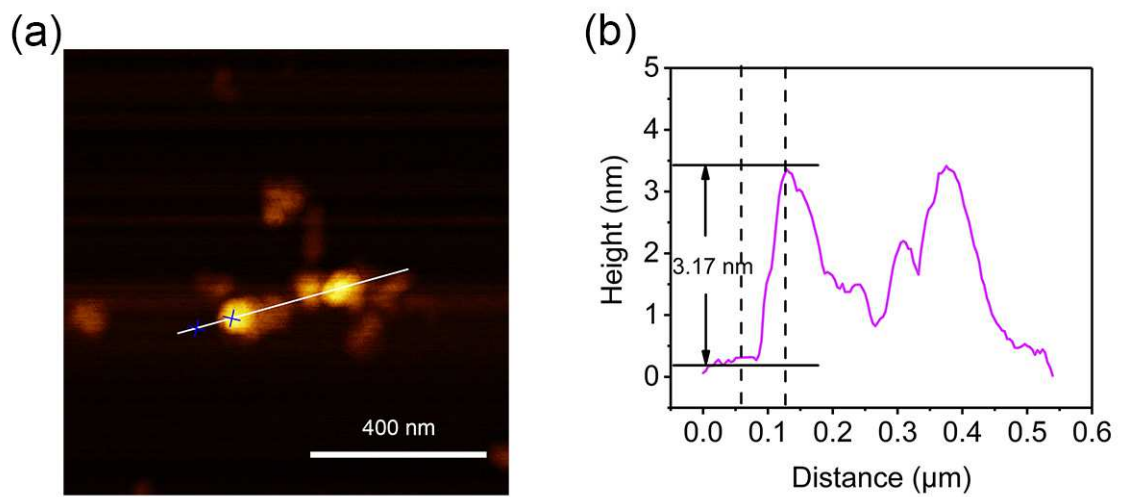


Fig. S2 AFM image (a) and corresponding height image (b) of MnO₂ NS dispersed on mica substrate.

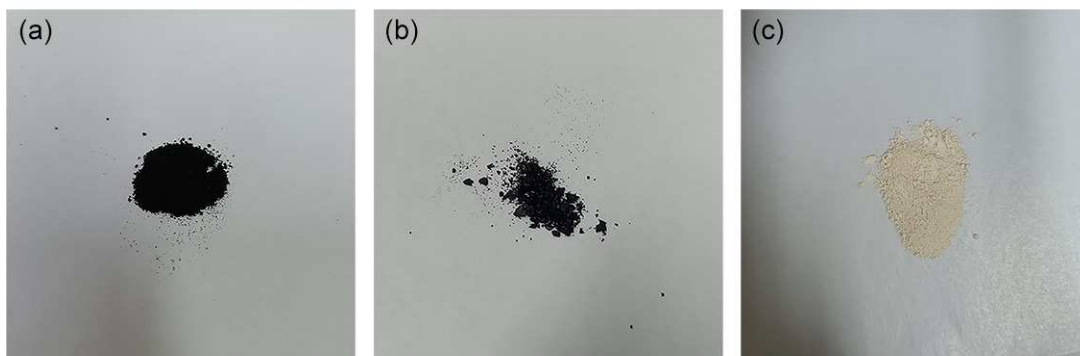


Fig. S3 Digital photos of (a) MnO_2 NS (b) MnO_2 -TCPP and (c) CaO_2 NP solid freeze-dried powder samples.

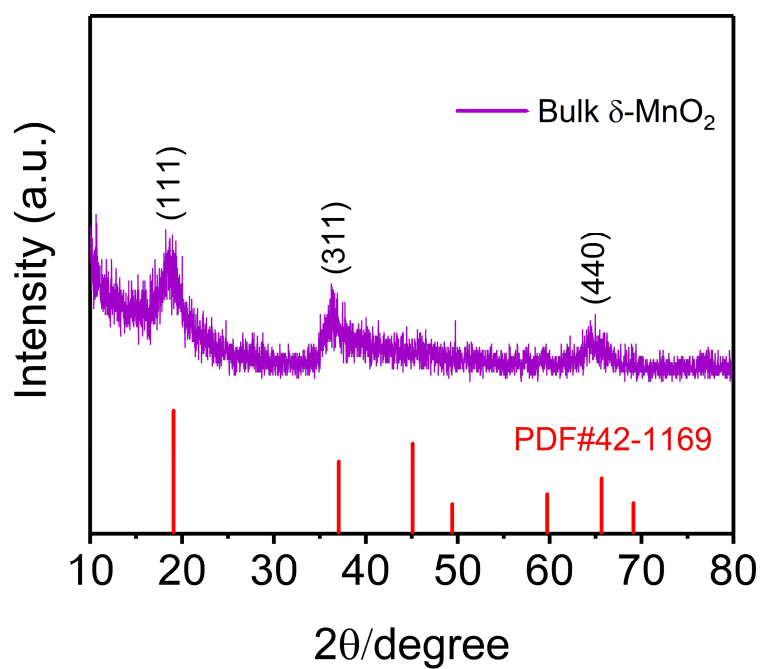


Fig. S4 XRD pattern of bulk $\delta\text{-MnO}_2$.

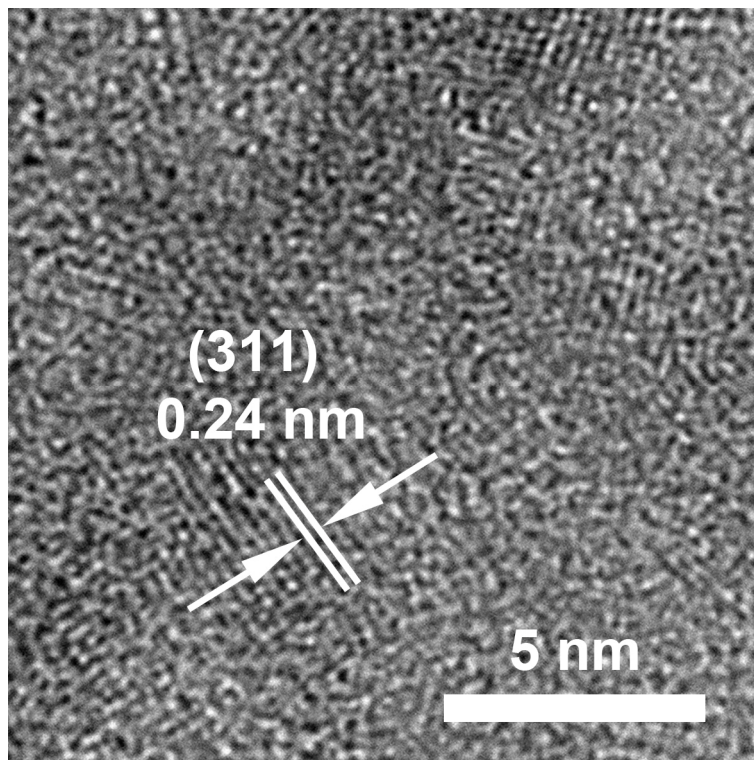


Fig. S5 HRTEM image of MnO₂ NS.

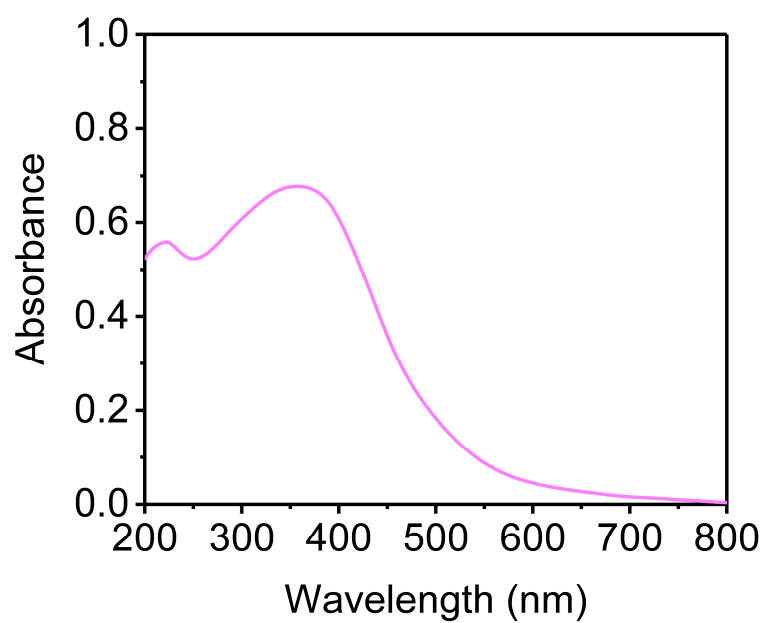


Fig. S6 UV-Vis-NIR spectrum of MnO₂ NS.

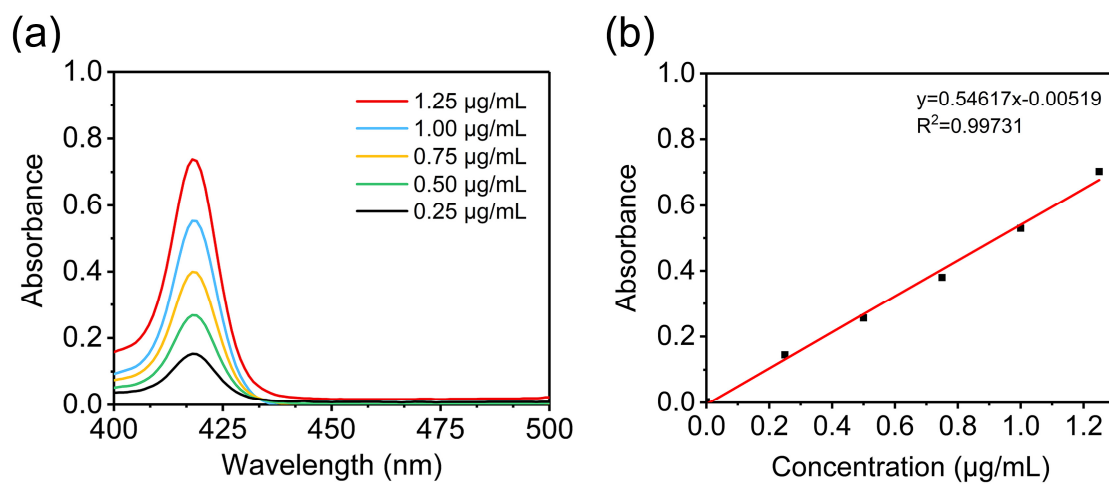


Fig. S7 (a) The absorbance curve of TCPP at various concentration. (b) The standard curve of TCPP was obtained from the absorbance at 419 nm.

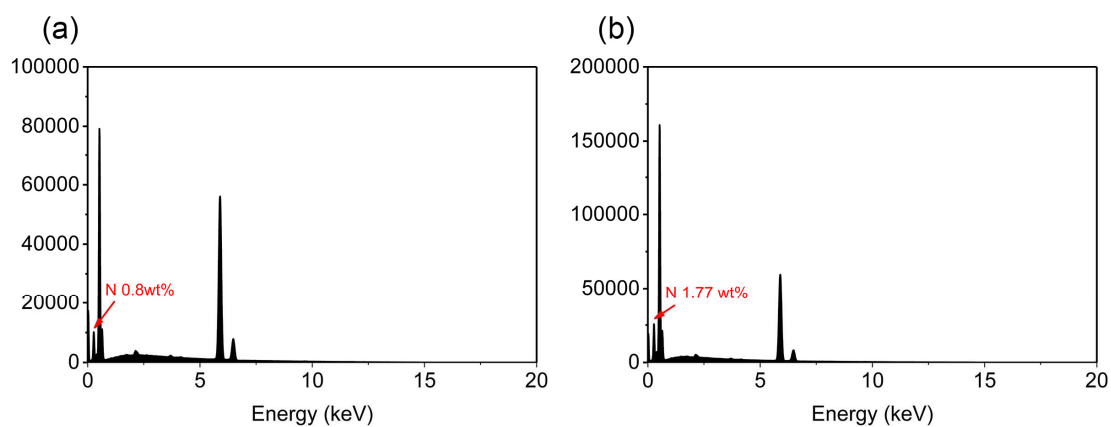


Fig. S8 EDS spectra of (a) MnO₂ NS and (b) MnO₂-TCPP.

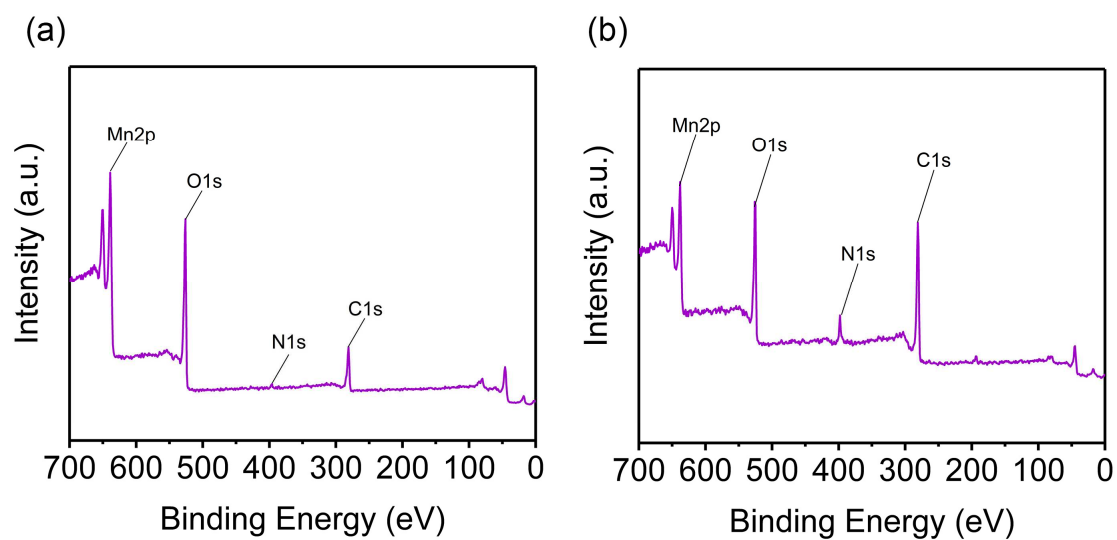


Fig. S9 XPS spectra of (a) MnO₂ NS and (b) MnO₂-TCPP.

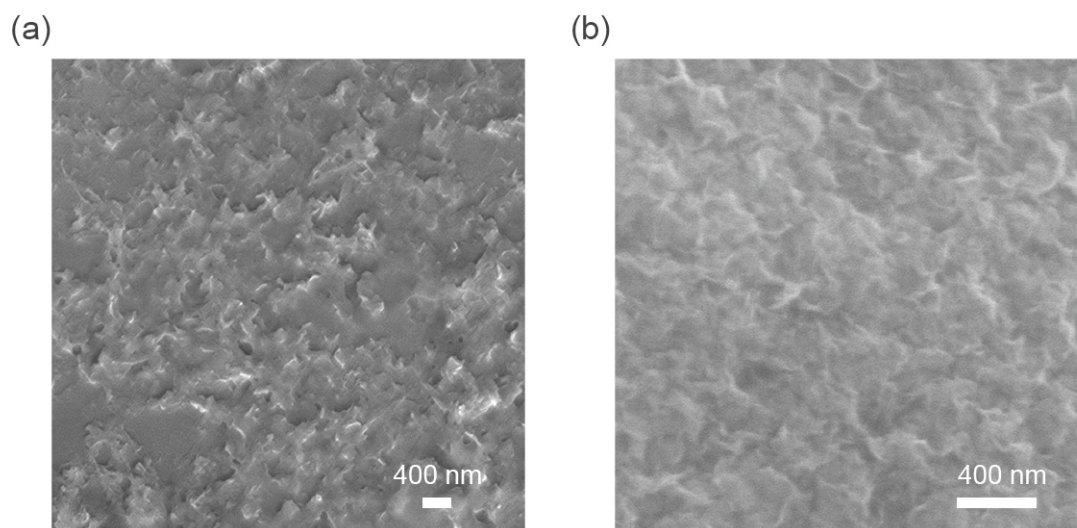


Fig. S10 SEM images of (a) MnO₂ NS and (b) MnO₂-TCPP.

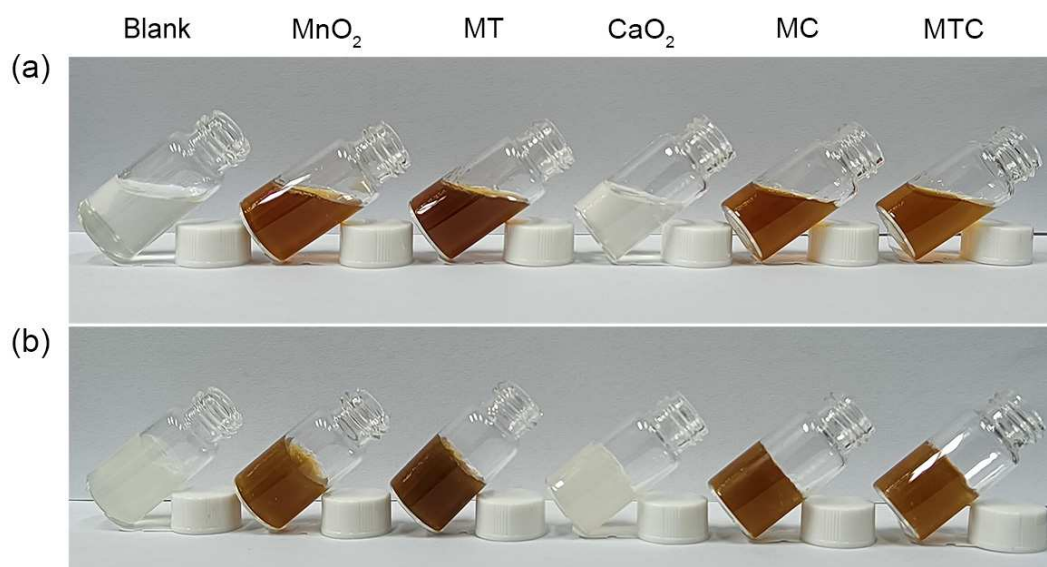


Fig. S11 Digital images of the sol-gel phase transition process for the preparation of MTC gel (doped with MnO₂-TCPP and CaO₂ NP). Photographs of process for the preparation of MTC hydrogels (a) before and (b) after adding the calcium ions.

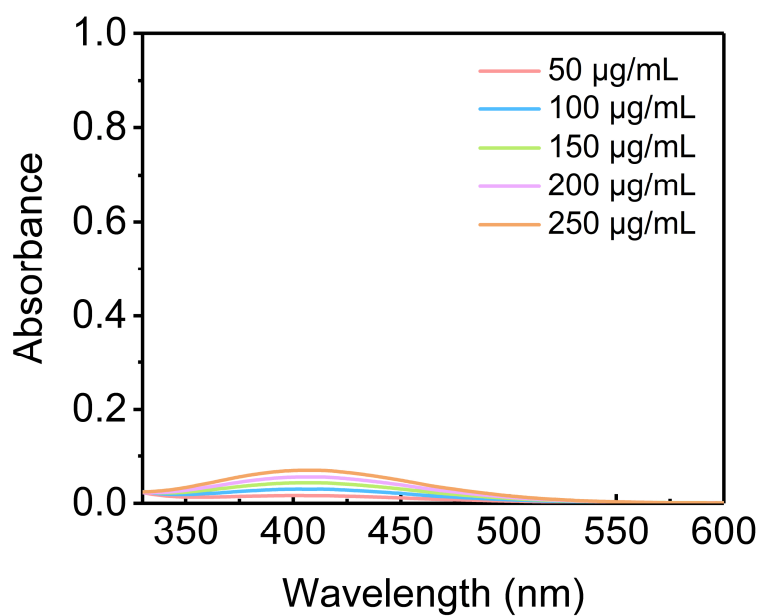


Fig. S12 H₂O₂ produced from various concentration of CaO₂ NP at pH 7.4 for 6 h.

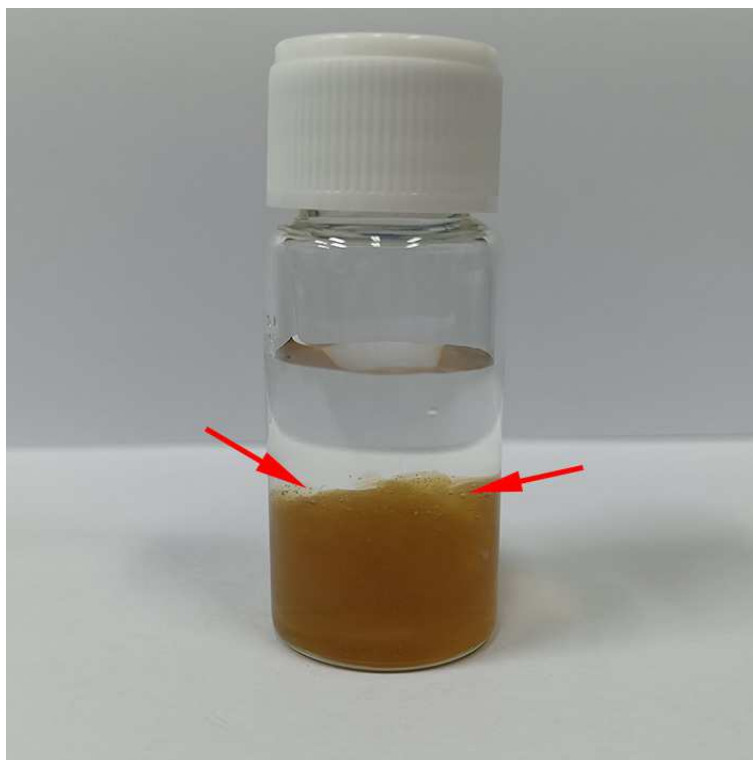
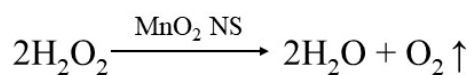
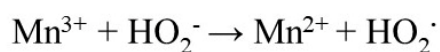


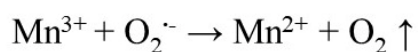
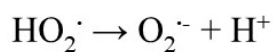
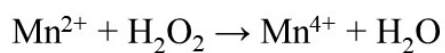
Fig. S13 Digital image of oxygen bubbles generated by MTC gel at 10 min. Red arrows showed some bubbles.



Initiation:



Chain propagation:



Chain termination:

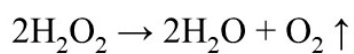
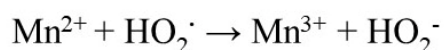


Fig. S14 The catalytic mechanism of MnO₂ NS as a catalase mimic to produces oxygen.

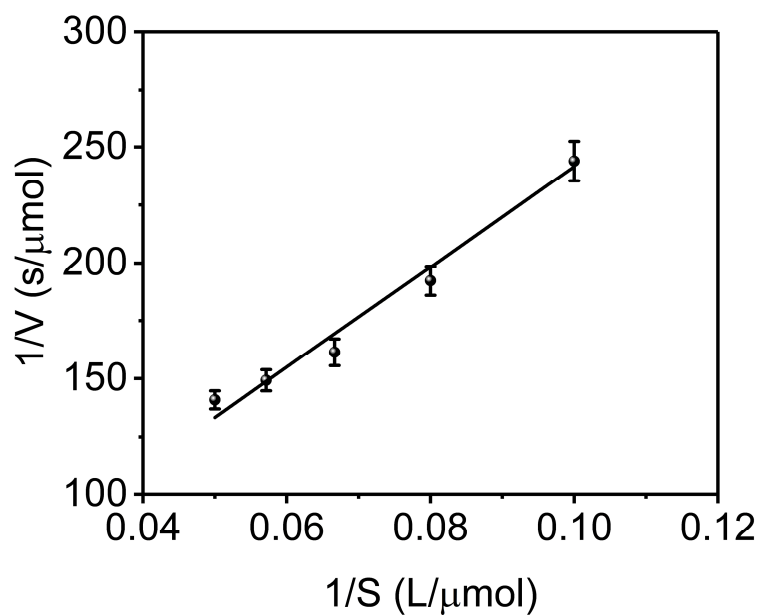


Fig. S15 Steady-state kinetic assay with 100 $\mu\text{g}/\text{mL}$ MnO_2 NS. Lineweaver-Burk plot of CAT-like activity of MnO_2 NS in the presence of various concentrations of H_2O_2 .

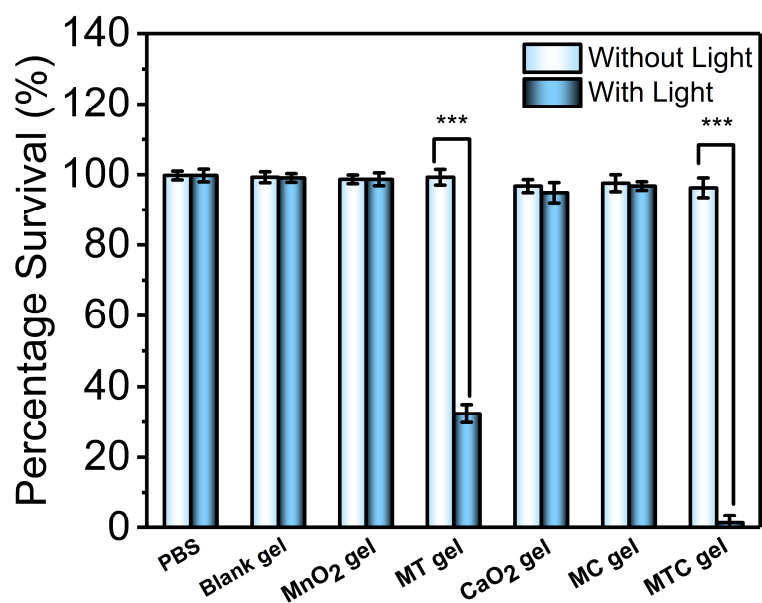


Fig. S16 Bacterial viability of *E. coli* after treating with Blank gel, MnO_2 gel, MT gel, CaO_2 gel, MC gel, MTC gel with or without Light ($0.65 \text{ W}/\text{cm}^2$, 10 min, $n = 3$, $*P < 0.05$, $**P < 0.01$, $***P < 0.001$).

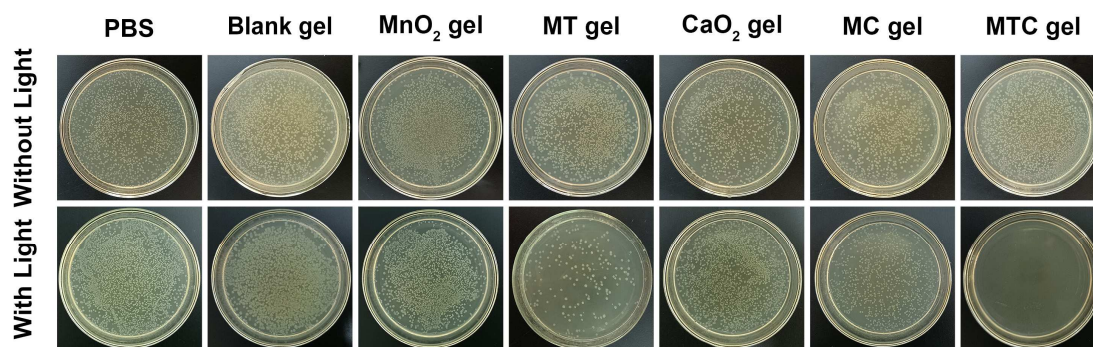


Fig. S17 Colonies of *E. coli* cultured on agar plates after various treatments.

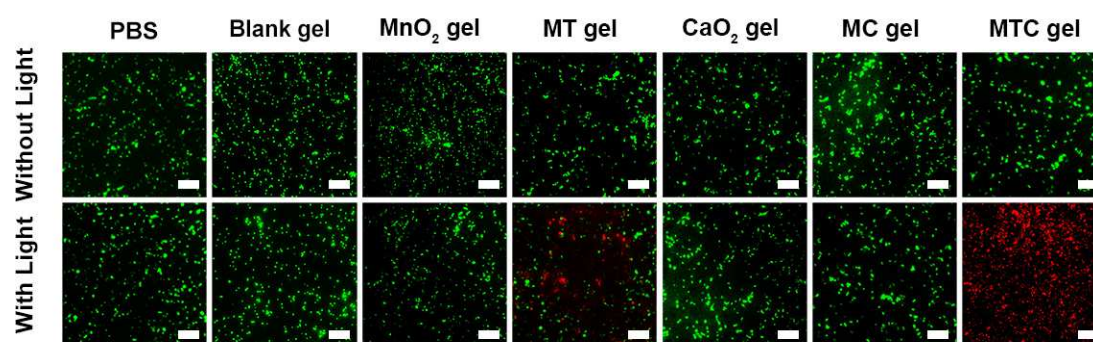


Fig. S18 Live/dead fluorescence images of *E. coli* stained by FDA (green, viable bacteria) and PI (red, dead bacteria) after various treatments. Scale bar: 20 μ m.

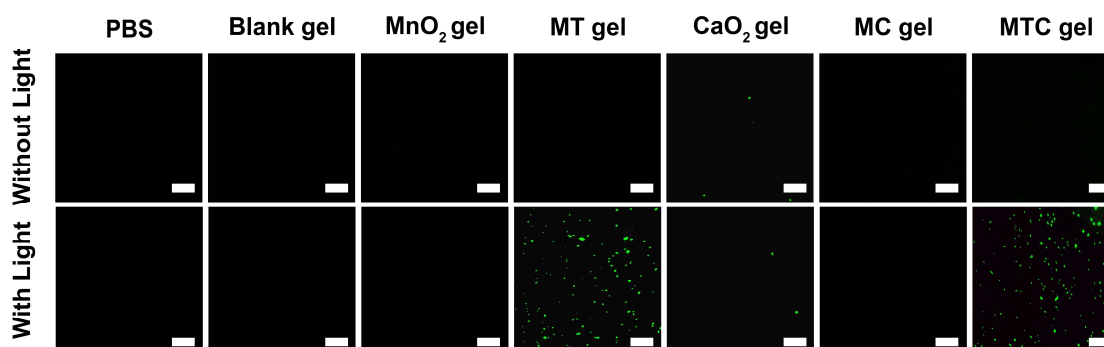


Fig. S19 Intracellular ROS fluorescence images (green) of *E. coli* stained by DCFH-DA after various treatments. Scale bar: 20 μ m.

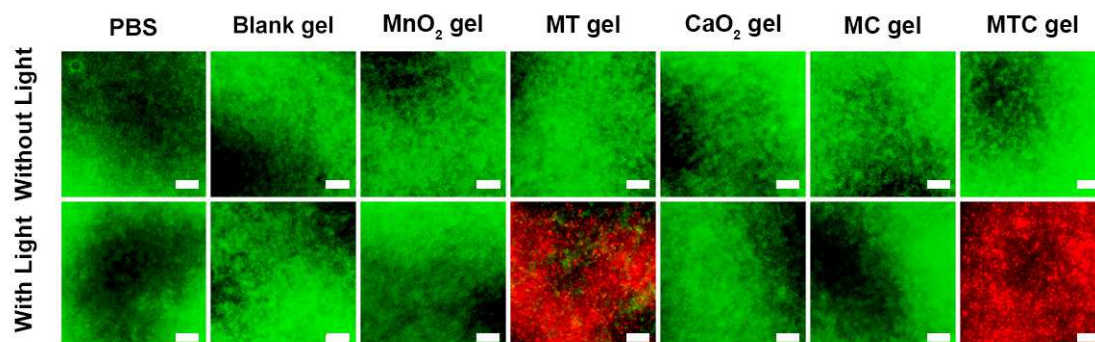


Fig. S20 Live/dead fluorescence images of *S. aureus* stained by FDA (green, viable bacteria) and PI (red, dead bacteria) after various treatments. Scale bar: 20 μm .

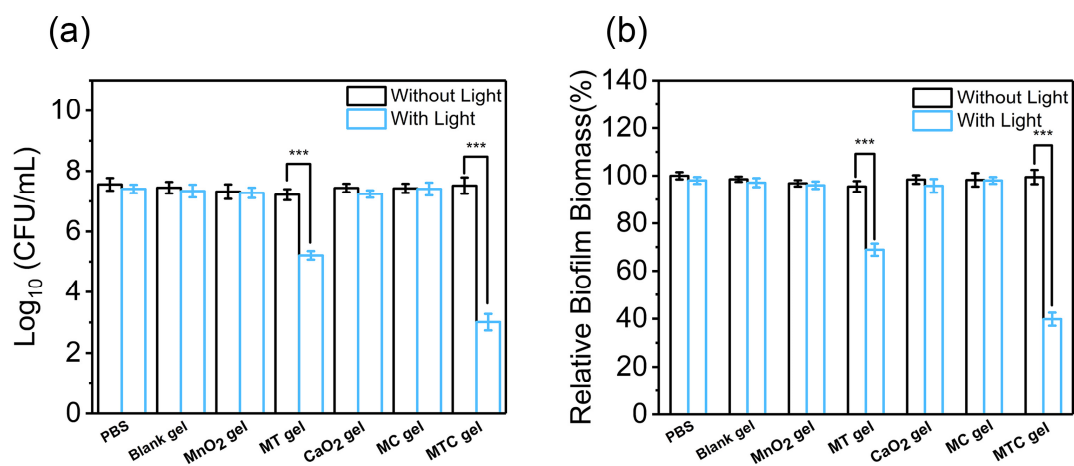


Fig. S21 (a) Numbers of viable *E. coli* in biofilms after various treatments. (b) Relative biofilm biomass of *E. coli* biofilm after various treatments ($n = 3$, $*P < 0.05$, $**P < 0.01$, $***P < 0.001$).

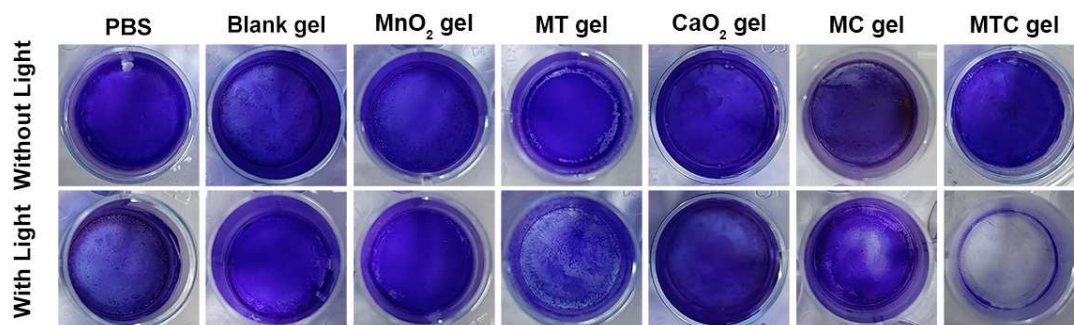


Fig. S22 Photographs of *E. coli* biofilm stained by crystal violet after various treatments.

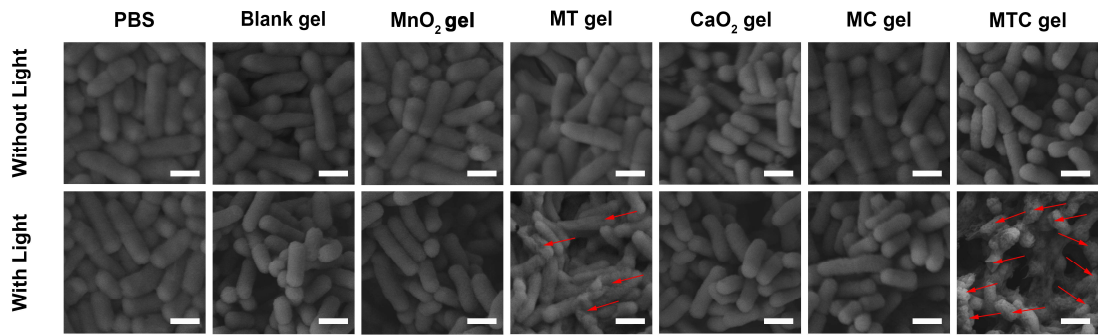


Fig. S23 SEM images of *E. coli* biofilm after various treatments. Red arrows show morphological damage of bacteria in biofilm. Scale bar: 1 μm .

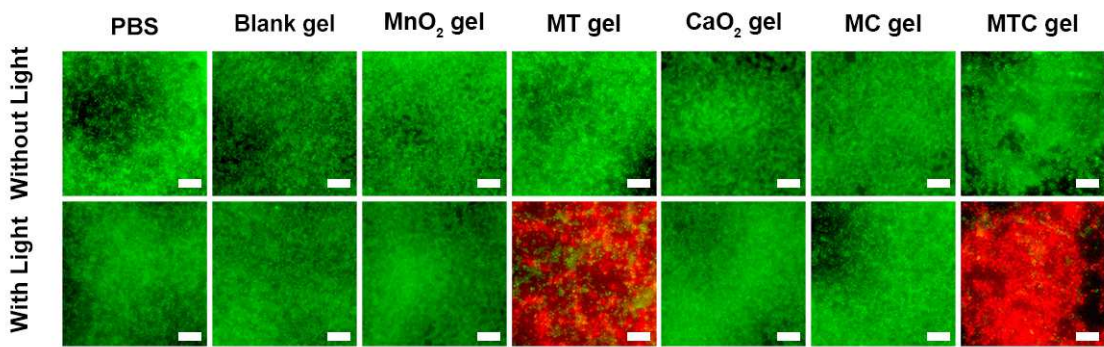


Fig. S24 Live/dead fluorescence images of *E. coli* biofilm stained by FDA (green, viable bacteria) and PI (red, dead bacteria) after various treatments. Scale bar: 20 μm .

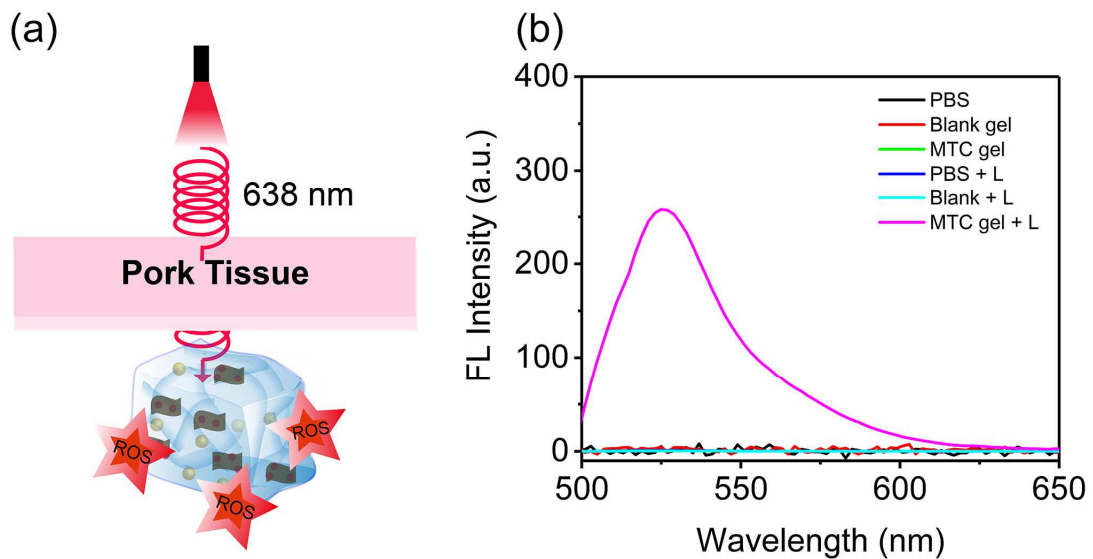


Fig. S25 (a) Illustration of in-deep tissue irradiation using 1 mm of pork tissue. (b) Fluorescence spectrum of DCF after treating with various groups through 1 mm of pork tissue with or without 638 nm light irradiation (0.65 W/cm^2 , 600 s).

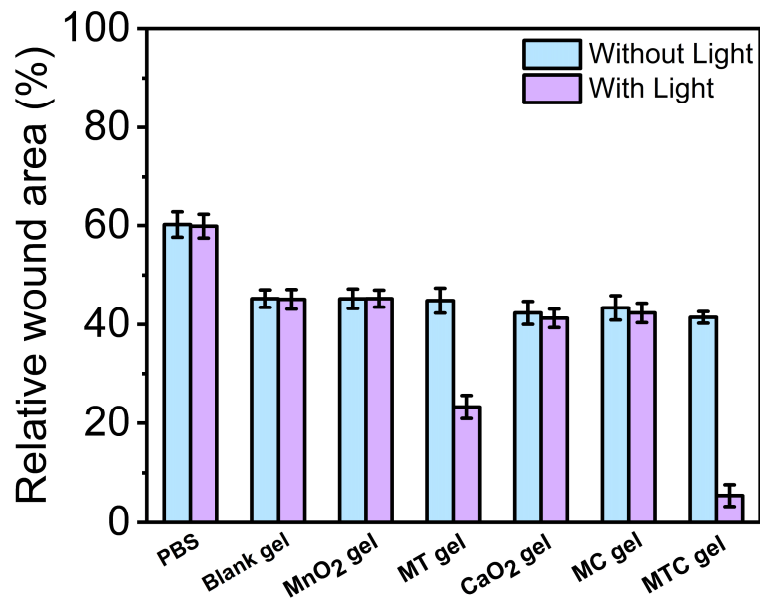


Fig. S26 Relative infected wound areas after a 12 days post-treatment (n=5).

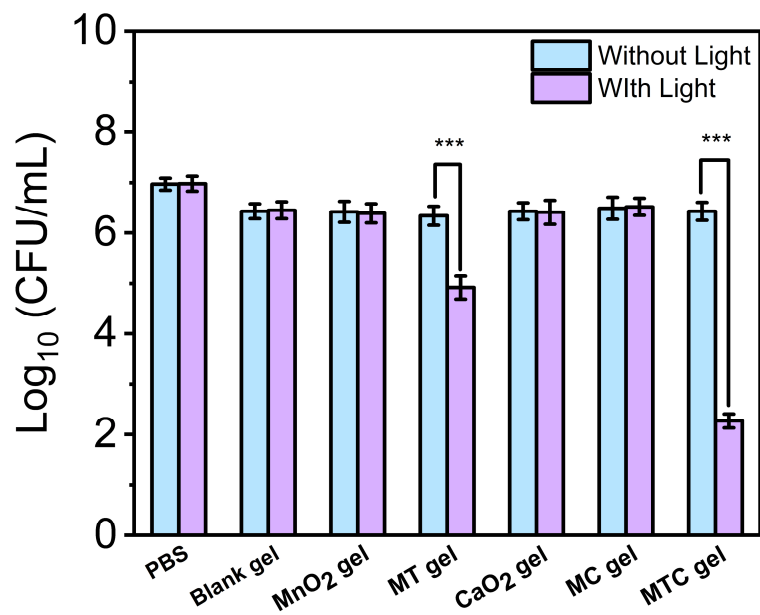


Fig. S27 Bacterial viability from biofilm-infected tissues after a 12 days post-treatment (n = 3, * $P < 0.05$, ** $P < 0.01$, *** $P < 0.001$).

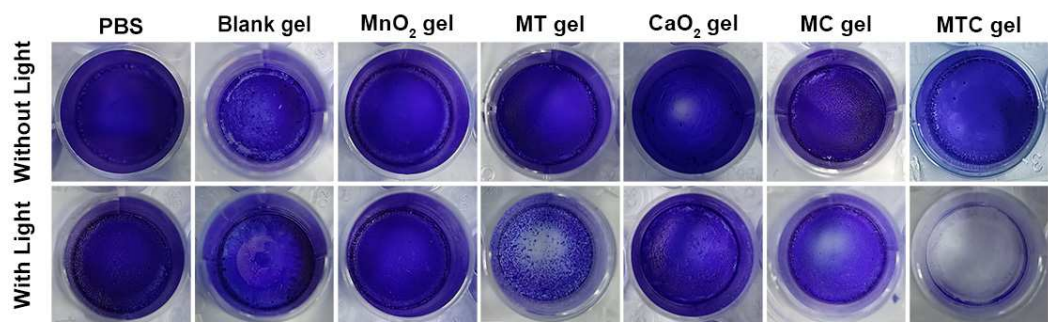


Fig. S28 Photographs of various stained biofilm of wound tissue rinsed by ethanol and placed in a 24-well plate.

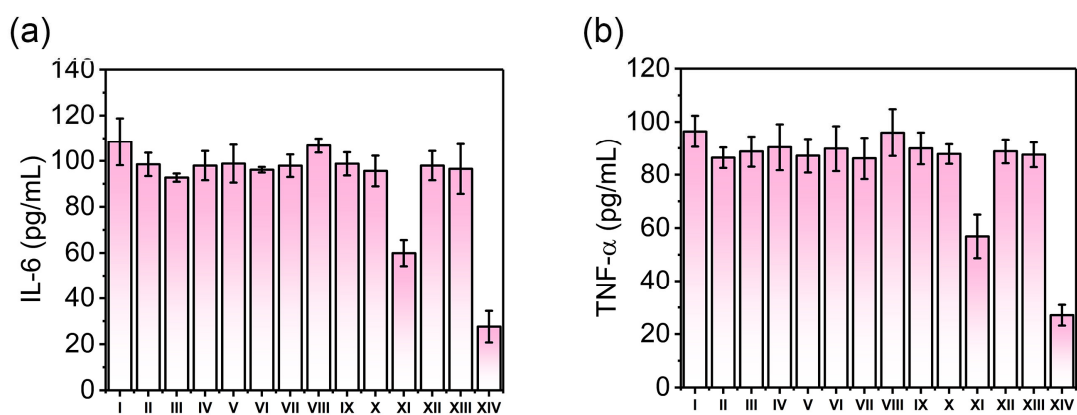


Fig. S29 Inflammation level assessment *in vivo* with ELISA detection of inflammation markers (IL-6 (a) and TNF- α (b)) after different treatments. (I) PBS, (II) Blank gel, (III) MnO₂ gel, (IV) MT gel, (V) CaO₂ gel, (VI) MC gel, (VII) MTC gel, (VIII) PBS + Light, (IX) Blank gel + Light, (X) MnO₂ gel + Light, (XI) MT gel + Light, (XII) CaO₂ gel + Light, (XIII) MC gel + Light and (XIV) MTC gel + Light (n=3).

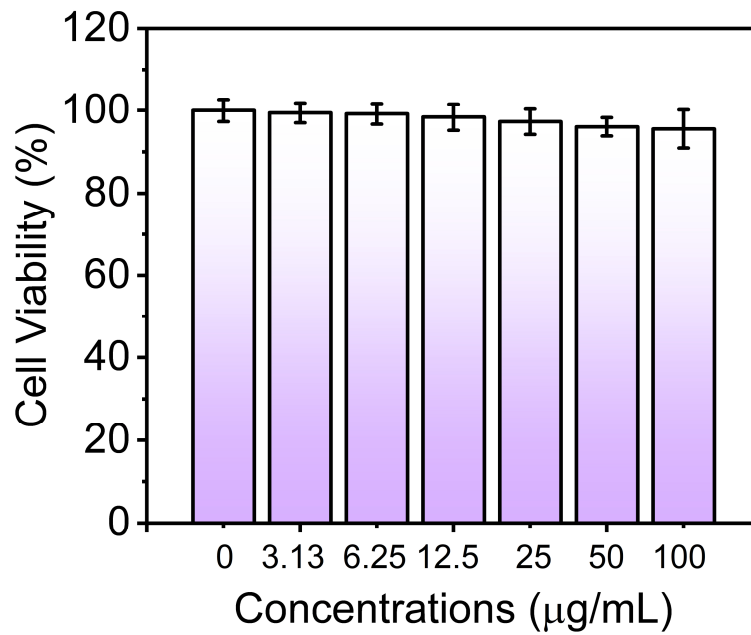


Fig. S30 The cell cytotoxicity of L929 cells after incubating with the leachate from MTC gel (containing different content of MnO₂-TCPP) for 4 h (n=3).

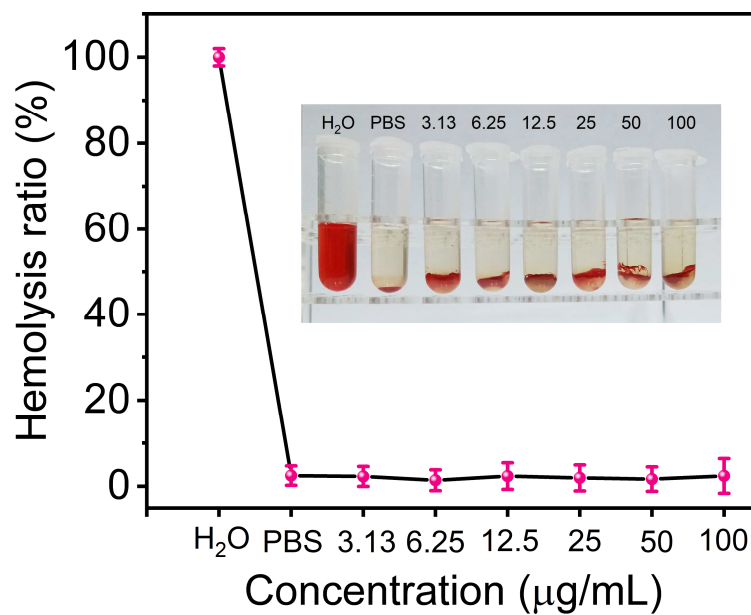


Fig. S31 Hemolysis ratio of RBC after incubating with water, PBS or hydrogels containing different concentrations of MnO₂-TCPP. The concentrations of MnO₂-TCPP are 3.13, 6.25, 12.5, 25, 50 and 100 µg/mL, respectively (n =3).

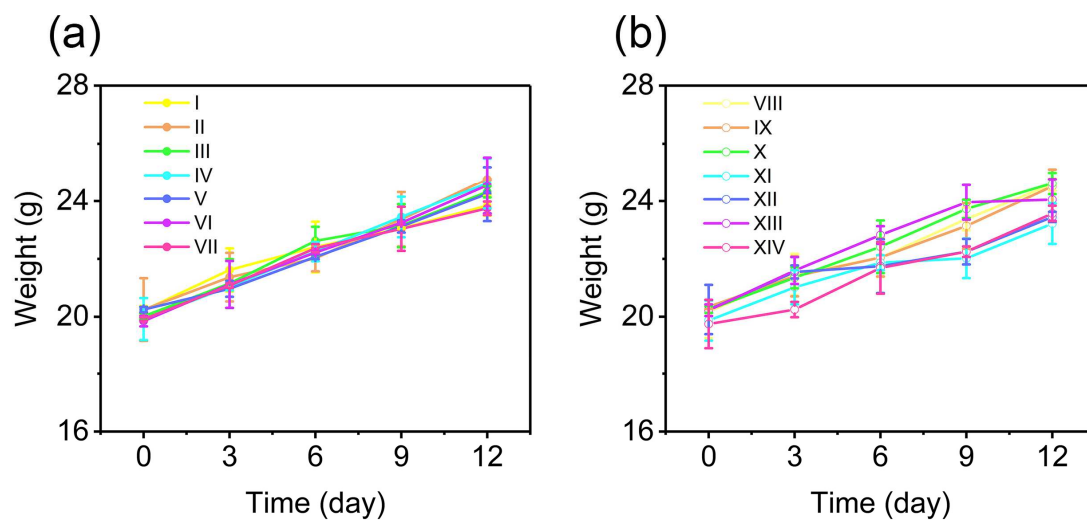


Fig. S32 Body weight changes of mice in different treatment groups. (a) (I)PBS, (II) Blank gel, (III) MnO₂ gel, (IV) MT gel, (V) CaO₂ gel, (VI) MC gel, (VII) MTC gel. (b) (VIII) PBS + Light, (IX) Blank gel + Light, (X) MnO₂ gel + Light, (XI) MT gel + Light, (XII) CaO₂ gel + Light, (XIII) MC gel + Light and (XIV) MTC gel + Light (n =5, **P* < 0.05, ***P* < 0.01, ****P* < 0.001).